Fuel 117 (2014) 1281–1287

Contents lists available at ScienceDirect

Fuel

journal homepage: www.elsevier.com/locate/fuel

Fusion and transformation properties of the inorganic components in biomass ash

Shenglei Du, Haiping Yang *, Kezhen Qian, Xianhua Wang, Hanping Chen

State Key Laboratory of Coal Combustion (Huazhong University of Science and Technology), Wuhan 430074, Hubei Province, China

HIGHLIGHTS

- Comprehensive transformation of inorganic components was studied by multi-means.
- Crystalline structure transformation of different biomass ashes was in-depth explored.
- Systematical analysis using phase diagrams was conducted to get the real fusion property of biomass ash.

ARTICLE INFO

Article history:
Received 3 March 2013
Received in revised form 19 July 2013
Accepted 19 July 2013
Available online 5 August 2013

Keywords:
Biomass ash
Transformation properties
Fusion characteristic
Phase diagrams

ABSTRACT

In thermochemical utilization of biomass, ash fusion temperature is an important parameter for the efficient and continuous operation of boilers/gasifiers and high value-added utilization of the ash. Fusion characteristics and transformation properties of the inorganic components in biomass ash are investigated using X-ray fluorescence (XRF), thermal gravimetric analyzer (TGA), X-ray diffraction (XRD), ash melting point test system and phase diagrams. XRF and TGA results show the changes of ash content, elemental composition and performance with the variation of temperature. Two main weight loss routes of biomass ash, decomposition and volatilization, are identified. XRD results show the transformation behavior of crystalline structure of different biomass ash. Intense internal reactions that occur in biomass ash at higher temperature generate a large amount of eutectic compounds, which lowered the melting point significantly. The contribution of different ash compositions to fusion can be assessed by binary diagrams while the fusion properties of silica-rich biomass ashes obtained by phase diagrams could be appropriate for industrial running.

1. Introduction

In the past decades, there has been renewed interest in biomass as an energy source due to the shortcomings of existing fossil fuel energy sources such as greenhouse gas emissions and other harmful effects on the environment [1,2]. Among different bio-energy conversion routes, which are determined by the demand and supply of available types and quantities of biomass, combustion and gasification are the most popular processing technologies [3]. But it is annoying that biomass contains various forms of alkali and alkali earth metals (AAEMs) and considerable amount of silica [4]. As a result, the biomass ash is easy to melt and volatilize [5,6]. So during the combustion or gasification processing, the ash with complex composition and high volatility often leads to slugging, defluidization and erosion/corrosion in thermal convention processing systems [7,8]. In order to improve the operational efficiency of boilers/gasifiers and achieve high value-added utilization of biomass ash, the study of fusion and transformation properties of inorganic elements in biomass ash has been an important issue in the past years.

A number of studies have been carried out so far to investigate the properties of biomass ash through experiment and simulation [4–14]. Niu et al. [9] found that to evaluate biomass ash fusion characteristics the melting characteristics indexes of coal quality for the eutectic compounds formation at high temperature should not be used. Other studies show that the ash-melting temperatures of some cereal grains are lower than 700 °C [11]. But usually, the ash-melting temperature measured by traditional ash melting point testing system cannot faithfully reflect the actual biomass ash fusion characteristics in industrial operations, causing many problems in thermal convention processing systems, especially in biomass-feeding boilers. Thy et al. [12] found that ash with less than 47 wt.% SiO_2 showed significant alkali metal loss. It was also found that ash with higher contents of SiO_2 would retain alkali metal in the melt and crystalline structures, mainly due to the prone reactions between alkali compounds and SiO_2, which stopped the volatilization of alkali chlorides. Direct experimental melting

---

* Corresponding author. Tel.: +86 27 87542417; fax: +86 27 87545526.
E-mail address: yhping2002@163.com (H. Yang).

0016-2361/$ - see front matter © 2013 Elsevier Ltd. All rights reserved.
http://dx.doi.org/10.1016/j.fuel.2013.07.085

studies were carried out to better understand the phase equilibrium and melting behavior of biomass ash [5,13], but so far the research is not comprehensive enough. Although predictive models utilizing equilibrium have been developed [11,15,16], little is known about the high temperature phase relations and the physical and chemical properties of the condensed phases.

Since biomass ash and silicate raw materials are similar in metal oxides composition and high-temperature environment, the phase diagrams from conventional silicate ceramics industry are also used for the analysis of ash fusion characteristics. Huggins et al. [17] used ternary diagrams of SiO_2–Al_2O_3–MO (M represents Fe, Ca, and K_2) to test the coal ash fusibility. But as to biomass ash, there is no systematic analysis by phase diagrams yet. Llorente et al. [18] compared five laboratory methods (fusibility, viscosity and utilization of appropriated phase diagrams, etc.) for predicting the ash sintering during the combustion of biomass to find an accurate and convenient way to evaluate the ash sintering behavior. But the conclusion was drawn only by a single ternary phase diagram of SiO_2–CaO–K_2O, which is not convincing. More diagrams should be employed to better understand the melting mechanism of the complex-composition ash.

Current methods for predicting and preventing fouling and slag deposition are mostly empirical and limited in theoretical analysis. It is necessary to explore the in-depth mechanism for biomass ash fusion characterization. In this study, the fusion characteristics of different biomass ashes are evaluated using XRF, TGA, XRD and ash melting point test system, followed by the systematic utilization of phase diagrams. The comprehensive study of ash transformation behavior was conducted and a new method of ash fusion characteristics evaluation by phase diagrams was proposed. The research findings will be helpful for improving the operational efficiency of biomass-feeding plants in industrial scale.

2. Samples and experimental methods

2.1. Samples

A total of 11 numbered biomass samples are prepared as shown in Table 1. The samples were pulverized and sieved with a 0.45 mm sieve. The results of the proximate and ultimate analysis are listed in Table 1.

The samples can be classified as follows:

Herbaceous biomass: cotton stalk, corn stalk, rape straw, wheat straw, rice straw, tobacco stem. The annual herbaceous biomasses also can be divided into two sub categories. One is soft straw with high ash content (~10%), e.g., wheat straw and rice straw. The other is gray straw with relatively lower ash content and property analogous to woody biomass, e.g., cotton stalk.

Woody biomass: pine, poplar, bamboo. The main feature of woody biomass is its low ash content, about 1%.

Chaff biomass: rice husk, peanut shell. The two chaff biomasses differ remarkably. The rice husk has the ash content as high as 16.8% while the peanut shell only 1.5%.

Table 1
Ultimate and proximate analysis of the samples.

No.	Samples	Ultimate analysis (wt.%)					Proximate analysis (wt.%)			
		N	C	S	O[a]	H	M_{ad}	V_{ad}	A_{ad}	FC_{ad}
1	Cotton stalk	1.2	45.2	0.3	46.9	6.3	5.1	73.0	3.1	16.7
2	Corn stalk	1.2	42.7	0.3	49.6	6.2	5.0	70.2	8.3	16.6
3	Rape straw	0.8	44.9	0.2	47.5	6.6	5.5	74.3	6.3	13.9
4	Wheat straw	0.6	40.4	0.3	52.9	6.0	4.4	68.5	12.9	14.2
5	Rice straw	0.9	37.5	0.1	42.8	5.9	5.0	82.1	7.7	5.1
6	Tobacco stem	2.6	36.1	0.8	55.6	4.9	3.6	68.5	21.7	6.1
7	Pine	0.1	51.0	0.0	42.9	6.0	15.3	70.4	0.2	14.2
8	Poplar	0.3	41.4	0.3	39.1	5.3	6.8	79.7	1.3	12.2
9	Bamboo	0.3	48.4	0.1	45.2	6.1	4.6	72.8	0.7	21.7
10	Rice husk	0.5	48.6	0.1	55.4	5.5	6.3	60.4	16.8	16.6
11	Peanut shell	1.9	60.5	0.4	30.1	7.1	9.1	56.6	1.5	31.9

[a] By difference. ad: the analysis was based on air dried basis.

2.2. Experimental methods

Ashing temperatures were set at 450 °C, 600 °C (ASTM E 1755–01, Standard test method for ash in biomass), 815 °C (GB/T212–2008, Proximate analysis method for coal, China) and 1000 °C for the experiments. In particular, experiments were conducted at 450 °C and 1000 °C to investigate comparatively the transforming properties of inorganic elements in biomass ash.

Ashing process: 1 g of biomass sample in a corundum crucible is placed into a muffle furnace below 100 °C and then heated up to the final temperature at 10 °C/min. Finally, a constant temperature is maintained for a specified period to ensure complete ashing: 5 h for 450 °C, 4 h for 600 °C, 2.5 h for 815 °C, and 1.5 h for 1000 °C. The ash content was obtained from the average value of several ashing trials.

The experimental methods are described as follows:

(a) The composition of biomass ash obtained by XRF (EAGLE III, EDAX Inc., USA) was used for elemental determination. Each ash sample was scanned three times and the average value was used to minimize the error.
(b) A thermal gravimetric analyzer (Perkin Elmer-Diamond TG, USA) was used to study weight loss properties of ash. The sample of approximately 5 mg is heated from room temperature to 1400 °C at a constant heating rate of 10 °C/min with the carrier gas of air. Reproducibility of the apparatus was tested before the experiment.
(c) Ash content and elemental composition analysis can only reflect the apparent changes of elemental content in biomass ash. Further work is required to analyze the interactive reaction of inorganic elements and the change of crystal structure using XRD [19,20]. The crystalline compounds in ash were identified using XRD (X'Pert PRO, PANalytical B.V., Netherlands). Peak identification was performed using High Score Plus software package.
(d) Fusion temperature test of biomass ash was conducted using a sintering instrument (Cabolite, UK). The heating process is observed and photographed using a high definition video camera in the atmosphere of air. The test is based on the changes in shape detected during the heating of the ash cone from 700 °C to 1500 °C under the heating rate of 10 °C/min and the storage interval is 2 °C. The four feature temperatures are recorded by computer, including deformation temperature (DT), softening temperature (ST), hemisphere temperature (HT) and flow temperature (FT). The experiment was conducted after verifying the reproducibility of the apparatus.

3. Results and discussion

3.1. Inorganic elements loss of ash

The results of XRF analysis are listed in Table 2. The main ash compositions are K, Na, Mg, Al, Ca, P, etc. in forms of oxides, silicates or chlorides [21], but the contents of the individual elements in different ashes differ significantly, which lead to great variance in performance.

It can be seen that with the increase of ashing temperature, the ash content drops straightly, especially at higher temperature (e.g., 1000 °C). Furthermore, the relative contents of K, Na and Cl also de-

Table 2
XRF results of ashes obtained under different temperatures.

Samples	Ashing temp. (°C)	Ash content[a] (%)	Na_2O	MgO	Al_2O_3	SiO_2	P_2O_5	SO_3	K_2O	CaO	Fe_2O_3	Cl
Corn stalk	450	11.1	0.4	2.2	1.6	36.3	4.3	3.7	29.4	6.1	0.8	15.0
	600	9.3	0.7	3.6	1.8	41.0	5.8	3.7	25.1	6.5	0.6	11.2
	815	8.8	0.6	3.7	2.8	45.2	8.5	4.6	21.4	9.6	0.9	2.0
	1000	6.7	0.6	2.4	2.0	45.8	4.3	9.2	17.7	14.7	0.8	2.3
Wheat straw	450	14.1	0.7	0.8	1.3	62.5	1.4	2.7	17.6	2.8	0.4	9.4
	600	12.9	1.1	1.0	1.5	53.8	2.8	3.7	21.3	4.2	0.6	10.1
	815	12.1	1.0	0.7	1.4	66.2	2.7	4.5	15.3	4.1	0.7	3.4
	1000	9.3	1.5	1.4	1.7	67.2	3.2	4.8	12.9	5.5	0.8	0.8
Rice straw	450	14.6	1.1	3.5	1.1	42.8	3.1	7.9	19.5	8.0	0.5	10.9
	600	12.7	1.0	2.3	0.9	52.0	2.5	6.5	17.8	7.7	0.8	7.1
	815	11.1	0.9	3.9	1.6	51.3	5.1	10.3	13.5	9.6	0.8	1.3
	1000	10.9	0.4	3.6	2.0	57.1	4.1	7.2	12.0	10.0	1.1	0.8
Poplar	450	2.9	0.8	3.4	5.4	38.2	5.7	5.8	10.5	26.1	2.9	0.6
	600	2.6	0.7	4.1	6.9	26.8	7.0	5.5	8.2	34.8	3.8	1.5
	815	2.2	0.7	5.2	5.1	29.2	9.0	8.7	9.2	27.4	3.0	1.1
	1000	2.0	0.8	3.4	7.1	29.6	6.5	10.0	5.7	32.3	3.1	0.6
Cotton stalk	600	2.9	2.4	6.4	5.8	18.2	7.1	9.5	17.1	26.1	3.8	2.8
	815	2.0	2.1	7.7	5.5	19.6	7.6	8.7	14.4	29.2	4.1	0.5
Rape straw	600	7.7	1.1	0.4	0.2	4.1	2.7	21.2	35.4	25.7	0.7	8.2
	815	6.2	0.9	1.5	1.2	3.3	2.3	25.2	32.4	25.2	0.7	6.9
Tobacco stem	600	17.3	0.4	5.9	–	0.1	4.1	8.0	21.2	31.4	0.1	28.2
	815	12.7	0.9	8.0	0.9	0.5	3.7	11.4	23.0	40.9	0.1	9.9
Pine	600	1.7	12.8	5.6	6.5	16.5	2.4	7.6	7.8	24.9	4.6	8.8
	815	1.4	12.6	7.7	6.3	17.2	2.7	10.3	5.5	26.6	3.3	4.9
Bamboo	600	0.9	–	4.5	–	19.2	6.4	8.2	49.2	6.0	3.1	1.1
	815	0.8	–	4.7	2.8	25.6	5.3	7.2	43.7	5.8	2.0	0.8
Rice husk	600	18.2	–	0.8	1.1	87.5	0.8	1.3	3.0	1.6	2.4	0.5
	815	18.2	–	0.6	0.9	91.3	0.7	1.0	0.5	2.4	0.2	1.1
Peanut shell	600	5.2	0.2	4.8	8.2	23.1	8.2	10.6	25.7	11.1	6.1	1.1
	815	4.6	0.2	5.4	7.8	24.1	8.9	11.5	24.0	11.3	4.9	0.6

[a] The ash content equals the mass of ash divided by the initial mass of biomass based on air dried basis.

crease. This indicates that the weight loss of ash is mainly because of the volatilization of K and Na in the form of chlorides [22]. The contents of Mg, Ca, Fe, Al and non-metallic elements S, P, and Si are increasing because of the decrease in ash content, suggesting that the compounds composed of these elements are relatively more stable or less volatile. In other words, the higher the content of alkalis, the greater the variation of ash content. For example, the ash content of rice husk changes very slightly with the variation of temperature because nonvolatile silica is the dominant ash content. The potassium-rich corn stalk ash decreases from 11.3% to 6.7%.

Along with the decrease of ash content, the appearance of ash also changes. For example, the herbaceous ashes, corn straw, wheat straw and rice straw, melt heavily under 1000 °C, while the poplar ash only shows loose crusting. Meanwhile, the ash color changes with the increase of temperature. It was found that ashes at lower temperature (450 °C) appeared dark gray, which might be attributed to the unburned char residue in ash. Ashes of 600 °C and 815 °C appeared light gray. When the temperature reached 1000 °C, some ashes appeared darker color again. For example, the color of rice straw ash varied from dark gray (450 °C) to light gray (600 °C), then to light purple at 815 °C and 1000 °C. It suggests that internal reactions occur in ash at high temperature, resulting in the formation of colored compounds. At the same time, most herbaceous biomass ash samples melt under 815 °C, while woody biomass ash samples do not. Therefore, compared with herbaceous biomass, woody and chaff biomass are more suitable as fuel in boilers.

The weight loss properties of biomass ash can be investigated by TG-DTG. Wheat straw ash and poplar ash were selected as typical herbaceous biomass and woody biomass, respectively. The weight loss curves are shown in Figs. 1 and 2. From Fig. 1 it can be found that the wheat straw ash shows quite different characteristics under various ashing temperatures. The total weight loss of the 600 °C ash sample is more than 30%, and a significant weight loss rate peak was found between 700 °C and 950 °C. The total weight losses of ash samples at 815 °C and 1000 °C are about 10% and 5% respectively, and there is no conspicuous peak under 950 °C. When the temperature exceeds 900 °C, the 600 °C sample and 815 °C sample show similar andante weight loss process, while the 1000 °C ash shows obvious weight loss only when the temperature is higher than 1050 °C. The weight loss property is determined by the composition of ash. KCl, the main volatile composition of wheat straw, plays an important role in the process. Taking into account others' studies [23,24], it indicates that the intense volatilization of alkali chloride (refer to Eqs. (1) and (2) below) occurs for the 600 °C ash from 750 °C to 950 °C. No weight loss peak was observed samples of higher ashing temperatures (815 °C and 1000 °C). The weight loss above 1000 °C may be attributed to the decomposition of relatively stable K-bearing species (e.g., Eq. (3) below) [8]:

$$\mathrm{KCl(s,l)} \rightarrow \mathrm{KCl(g)}\ (>700\,^{\circ}\mathrm{C}) \tag{1}$$

$$\mathrm{2KCl(s,l)} \rightarrow \mathrm{(KCl)2(g)}\ (>700\,^{\circ}\mathrm{C}) \tag{2}$$

$$\mathrm{K_2SO_4(s,l) + H_2O(g)} \rightarrow \mathrm{2KOH(g) + SO_2(g)} \uparrow + 1/2\mathrm{O_2(g)} \uparrow \tag{3}$$

As shown in Fig. 2, the performance of poplar ashes is similar to that of the wheat straw ashes. The 600 °C ash shows more remarkable weight loss than that of ash derived from 815 °C and 1000 °C. But

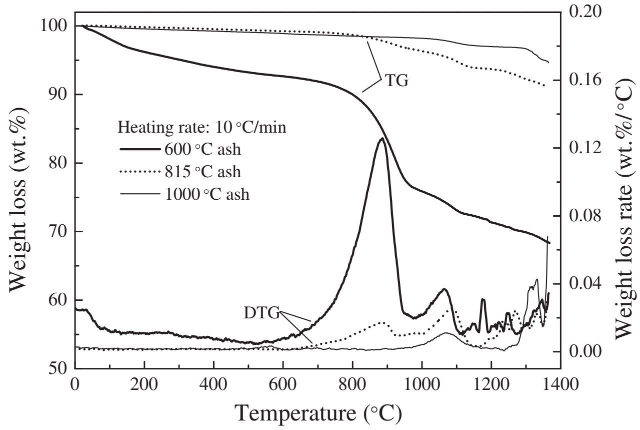

Fig. 1. TG–DTG curves of wheat straw ashes obtained under different temperatures.

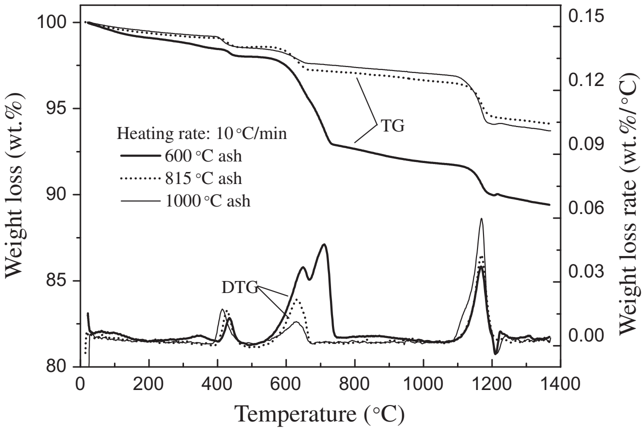

Fig. 2. TG–DTG curves of poplar ashes obtained under different temperatures.

there are also some differences. Compared with wheat straw ash, the poplar ash has a sharp loss in a relatively lower temperature range (600–750 °C). Considering the high calcium content in poplar ash, the sharp weight loss is mainly attributed to the decomposition of calcium carbonate (Eq. (4)). This weight loss route differs from that of the wheat straw ash. For poplar ash, calcium carbonate plays an important role, while potassium chloride is more crucial for wheat straw ash. Since there is nearly no weight loss from 800 °C to 1200 °C, the curves of 815 °C ash and 1000 °C ash almost overlap. Another difference is the 600 °C wheat ash has the maximum weight loss of 30% while for the poplar ash the maximum weight loss is only 10%.

$$CaCO_3 \rightarrow CaO + CO_2(g)\uparrow \tag{4}$$

The ash content, composition and performance changed significantly with the variation of temperature. Through comparison of ashes obtained under different temperatures, it is found that 600 °C is the most appropriate temperature for biomass ash analysis in industrial applications, because the 600 °C ash can not only characterize the ash content accurately, but also reflect the ash composition correctly. At 815 °C and 1000 °C, large amount of active elements evaporated, and the test results could not reflect the real content and composition of biomass ash. The 450 °C ash is able to accurately reflect the ash content of biomass and ash composition. Nevertheless, due to the great difference between the industrial practice and the ash preparation in the lab as well as the presence of residual unburned char in ash, 450 °C is also not suitable for biomass ash test.

3.2. Transformation of inorganic crystalline structure

Four ash samples, wheat straw, rice straw, corn stalk and poplar, were analyzed with XRD to study the transformation of crystalline structure. Fig. 3 shows the intuitive XRD spectrum results of corn stalk ashes obtained under different temperatures, which typically reflect the change of biomass ash crystalline structure with the variation of ashing temperature. Table 3 gives the main crystalline compounds in ashes.

It can be seen in Fig. 3 that the peak number of 450 °C ash and that of 600 °C ash are almost the same. But as to the peak intensity, the 600 °C ash is stronger than the 450 °C ash. It is mainly because that the peak intensity of 450 °C ash is weakened by the unburned char while the 600 °C sample is ashed completely. With the increase of ashing temperature, the peak number gradually increases, while the peak intensity decreases notably. In particular, diffraction peak intensity becomes very weak at 1000 °C. It means that complex reaction occurs dramatically within the ash, resulting in the formation of microcrystalline compounds, eutectic compounds or amorphous compounds at higher temperatures. Silica acts as a core reactant with other metal oxides or salts, like Eq. (5) [25]:

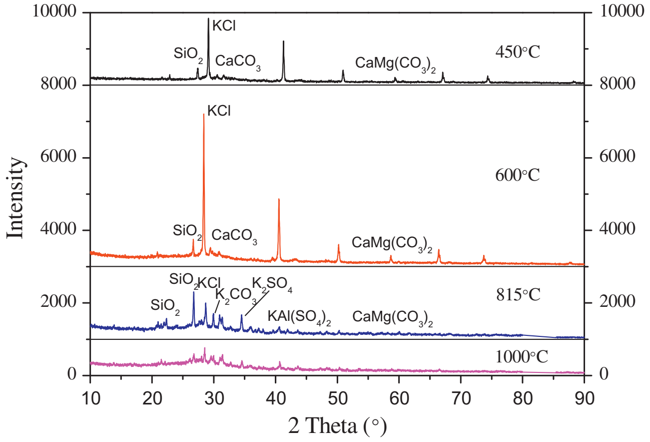

Fig. 3. XRD patterns of corn stalk ashes obtained under different temperatures.

Table 3
XRD results of ashes obtained under different temperatures.

Samples	Ashing temp. (°C)	Main components
Wheat straw	450	KCl; SiO_2
	600	$CaCO_3$; KCl; SiO_2; $CaMg(CO_3)_2$; $KAlSiO_4$
	815	SiO_2; K_2SO_4; $KAlSi_3O_8$
	1000	SiO_2; K_2SO_4; $KAlSi_3O_8$
Rice straw	450	KCl; SiO_2; $CaCO_3$; $CaMg(CO_3)_2$
	600	KCl; SiO_2; $CaCO_3$; $CaMg(CO_3)_2$; $K_2(SO_4)$
	815	KCl; SiO_2; $CaMgSi_2O_6$; Ca_2SiO_4 ; $K_2Ca_2(SO_4)_3$; $CaMg(CO_3)_2$
	1000	$CaMgSi_2O_6$; Ca_2SiO_4; K_2SO_4; $KAlSi_3O_8$
Corn stalk	450	KCl; SiO_2; $CaCO_3$; $CaMg(CO_3)_2$
	600	SiO_2; $CaCO_3$; KCl; $CaMg(CO_3)_2$; K_2CO_3
	815	SiO_2; K_2SO_4; K_2CO_3; $K_6Ca(SO_4)_4$; $KAlSiO_4$
	1000	CaO; $CaCO_3$; K_2SO_4; $CaAl_2Si_2O_8$; SiO_2; Ca_2SiO_4
Popar	450	SiO_2 $CaCO_3$ KCl CaO $K_2Ca_2(SO_4)_3$ CaP_2O_6
	600	CaO SiO_2 $CaCO_3$ $K_2Ca_2(SO_4)_3$ $KAlSi_3O_8$ Ca_2SiO_4
	815	CaO SiO_2 $K_2Ca_2(SO_4)_3$ $KAlSi_3O_8$
	1000	SiO_2 $CaSO_4$ $Ca_2P_2O_7$ $KAlSi_3O_8$ $KAlSiO_4$ Ca_2SiO_4 $K_2Ca_2(SO_4)_3$

$$2SiO_2 + Al_2O_3 + 2KCl + H_2O \rightarrow K_2O \cdot Al_2O_3 \cdot 2SiO_2 + 2HCl(g)\uparrow \quad (5)$$

From Fig. 3, it can be observed that KCl, $CaCO_3$, SiO_2 are the main crystalline compounds in lower-temperature ash (450 °C and 600 °C). Potassium mainly exists in the form of KCl. With the increase of temperature, the peak intensity of KCl gradually decreases or even reaches zero, suggesting that substantial proportion of KCl evaporates to the gas phase or converts into other compounds. It is consistent with previous XRF analysis. At higher temperature (815 °C), potassium mainly exists in the forms of $KAlSiO_4$, $K_2Ca_2(SO_4)_3$, $KAlSi_3O_8$ or other eutectic compounds by the route of Eq. (5). At 1000 °C, the eutectic compounds have been dominant in ash. Transformation properties of sodium are not reflected in the XRD results because of its low content. But with its property similar to potassium, the transformation behavior of sodium may be similar to that of potassium. Calcium mainly exists in the form of $CaCO_3$ at temperatures 450 °C and 600 °C. As the temperature increases (815 °C and 1000 °C), $CaCO_3$ gradually decomposes to CaO (Eq. (4)), and reacts with SiO_2 and other oxides, generating eutectic compounds of low melting temperature (Eq. (6)).

$$6SiO_2 + CaO + 2K_2CO_3 \rightarrow 2K_2O \cdot CaO \cdot 6SiO_2 + 2CO_2(g)\uparrow . \quad (6)$$

3.3. Ash fusion characteristic analysis with instrument and phase diagrams

As shown in Table 4, the ash fusion temperatures of prepared ash samples are measured using a conventional sintering instrument. It can be observed that all the deformation temperature (DT) of the ash increase with ashing temperature increasing. The maximum temperature difference (defined as the maximum value minus the minimum value) of DT is considerably large: 98 °C for the poplar ash and over 200 °C for the three herbaceous biomass ashes. But the maximum temperature differences of soft temperature (ST), hemisphere temperature (HT) and fluid temperature (FT) are smaller than that of DT. It is mainly due to the slow heating rate of the sintering instrument. Most of the active elements, Na, K, Cl, etc., evaporate with the slow heating process among 800–1000 °C [26]. It can be inferred that the ashes contain similar high-temperature molten materials which act as skeleton structure in biomass ashes [9]. The high-temperature molten material is not originally found in the ash, but formed during the slow heating process.

The ST is generally considered to be an important parameter in industrial operation. But the ST data obtained from industrial running boilers is usually 200 °C lower than the data from ash fusion characteristic test in laboratory [11]. Therefore, it is important to explore more accurate methods to evaluate the ash fusion properties. Biomass ash is the combination of silica and metallic oxides, which is very similar to the raw materials of conventional silicate ceramics industry. This provides a possible route to evaluate the biomass ash fusion characteristic based on the data from silicate ceramics industry.

The binary and ternary system phase properties of target system are tested under chemical equilibrium, eliminating the impact of volatilization or other reactions. Therefore, the phase diagrams can provide information of the fusion characteristics of target systems. This paper attempts to evaluate the biomass ash fusion characteristics by phase diagrams.

Table 4
Fusion temperature test of biomass ashes.

Samples	Ashing temp. (°C)	DT (°C)	ST (°C)	HT (°C)	FT (°C)
Corn stalk	450	800	1098	1218	1236
	600	784	1080	1156	1270
	815	904	1100	1222	1274
	1000	995	1102	1242	1276
Max. temp. difference	–	211	22	86	40
Wheat straw	450	766	1168	1278	1320
	600	770	1170	1272	1314
	815	806	1162	1260	1326
	1000	1006	1192	1226	1300
Max. temp. difference	–	240	30	52	26
Rice straw	450	742	1132	1254	1322
	600	748	1100	1200	1226
	815	876	1130	1184	1224
	1000	1020	1140	1196	1246
Max. temp. difference	–	278	40	70	98
Poplar	450	1040	1184	1200	1224
	600	1088	1184	1194	1206
	815	1114	1182	1188	1204
	1000	1138	1198	1204	1224
Max. temp. difference	–	98	16	16	20

The binary phase diagrams of SiO_2–XO (XO represents metal oxides) were employed firstly. The position of the ash in SiO_2–XO phase diagrams (the diagrams were referred from others' work [27,28]) was determined by the molar ratio of SiO_2/XO. As to the wheat straw ash, the melting point of the eutectic compound is 742 °C. Rice straw ash and corn stalk ash are similar to that of wheat straw due to the similar molar ratio of SiO_2/K_2O. But the rice husk ash is distinctly different from the previous ones in terms of fusion properties, because of the dominant silica content determining the melting point of rice husk ash. Even though the liquid is found at 769 °C, the amount of eutectic compound formed is not big enough to affect the overall fusion potential. The binary phase diagrams of silica were also compared with that of other oxides for the analysis of fusion contribution of the main elements in ash [28–31]. The contributions are listed here according to the melting temperatures:

$$Al_2O_3 > MgO > CaO > P_2O_5 > Na_2O > K_2O.$$

Therefore, the presence of Al_2O_3, MgO and CaO in ash may increase the ash melting point, while the presence of P_2O_5, Na_2O and K_2O play the contrary influence on melting point. So in industrial application, Al_2O_3-rich kaolin is often used as bed material in fluidized bed gasifier or boiler to avoid or mitigate agglomeration [32]. It is noteworthy that, besides sodium and potassium, the presence of phosphorus can also greatly reduce the melting point of ash. Hence some measures should be taken to reduce the phosphorus content for the P-rich biomass as boiler fuel.

The binary phase diagrams of silica with other oxides are clearly inadequate to evaluate the fusion characteristic of complex ash. The ternary system phase diagram is a good complement for this problem. According to the existing phase diagram of biomass ash composition ratio, the position of biomass ash in the phase diagrams can be determined, hence the melting temperature would be estimated, as shown in Fig. 4. The biomass ash melting points based on ternary system phase diagrams are shown in Table 5. The melting points of rape stalk and tobacco stalk ash cannot be determined due to the low SiO_2 content, because few studies are involved in silica-poor region since it is less useful in conventional silicate industry and difficult to practice in research.

As to the other 9 ash samples, the minimum values of melting temperature from respective phase diagrams (here without using

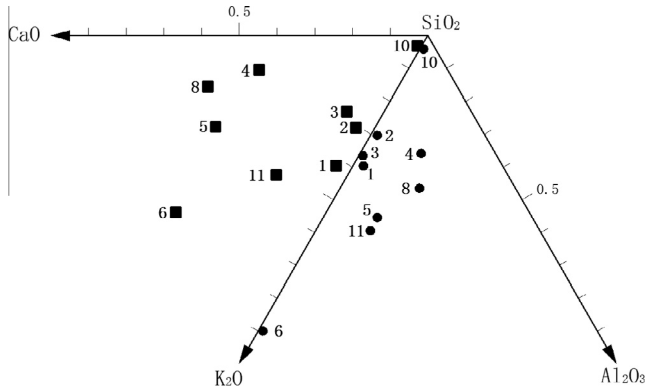

Fig. 4. Positions of ash samples in SiO_2–K_2O–CaO and SiO_2–K_2O–Al_2O_3 phase diagrams.

Table 5
Estimated values of biomass ash melting point from ternary system phase diagrams.

Samples	SiO_2 content (wt.%)	Melting point from ternary phase diagram (°C)					Minimum value (°C)
		Si–Mg–K	Si–Ca–K	Si–Fe–K	Si–Al–K	Si–K–Na	
Cotton stalk	18.21	1360 ± 10	>1500	910 ± 10	1500 ± 20	900 ± 10	900 ± 10
Corn stalk	40.97	900 ± 30	950 ± 10	750 ± 10	810 ± 20	740 ± 10	740 ± 10
Rape straw	4.05	–	–	–	–	–	–
Wheat straw	53.76	800 ± 20	875 ± 10	800 ± 15	720 ± 20	750 ± 10	720 ± 20
Rice straw	51.99	900 ± 30	920 ± 10	770 ± 10	760 ± 10	870 ± 10	760 ± 10
Tobacco stem	0.12	–	–	–	–	–	–
Pine	16.47	1480 ± 10	>1500	870 ± 10	>1500	900 ± 10	870 ± 10
Poplar	26.83	1050 ± 10	>1500	900 ± 10	1300 ± 10	900 ± 10	900 ± 10
Bamboo	19.22	–	–	–	–	780 ± 10	780 ± 10
Rice husk	87.47	>1500	>1500	>1500	>1500	769 ± 5	769 ± 5
Peanut shell	23.11	1380 ± 10	1260 ± 20	900 ± 10	1400 ± 10	780 ± 10	780 ± 10

"Si–Mg–K" stands for the SiO_2–MgO–K_2O ternary phase diagram.
"–" Indicates there is no suitable phase diagram to be used for reference.

the phase diagram of Si–Ca–Na data for the quite low sodium content in ash) were selected to evaluate the fusion properties of biomass ash. The minimum melting temperature derived from the single phase diagram partially reflects the fusion potential. Based on minimum temperature of the biomass ash besides rice husk, it can be derived that the melting points are about 700–900 °C, which are consistent with the data from actual operation [11]. The three herbaceous biomass ash samples and peanut shell ash have the melting points of about 750–800 °C. The woody biomass ash and some herbaceous ash with similar composition such as cotton stalk ash have the melting points of about 900 °C. The results derived from the phase diagrams reflect the melting characteristics of biomass ash more accurately [33].

But as to the rice husk ash and bamboo ash, the results seem not ideal. The melting point of rice husk ash is usually more than 1200 °C, which is quite different from the minimum value, i.e., 769 °C. That is because the fusion property of ash is also affected by the amount of eutectic compounds. If the amount of low-melting-temperature eutectic compounds is too small, the dominated influence is weakened.

As shown in the above analysis, it is convenient to analyze the fusion characteristic of most biomass ashes using silicate ternary phase diagrams. Despite some limitations, e.g., chlorine cannot be reflected in the phase diagrams and the silica-poor ash is difficult to analysis, this approach is important for analysis of biomass ash fusion characteristics.

4. Conclusions

The characteristics of different biomass ashes were investigated using XRF, TGA, XRD and ash melting point test system. And the phase diagrams were employed to provide useful information for better understanding of different fusion characteristics of biomass ashes.

The ash content, composition and performance change with the variation of temperatures. There are two main weight loss routes of biomass ash: decomposition and volatilization. Through comparison of ashes obtained under different temperatures, it is found that 600 °C is the most appropriate for ash analysis in industrial applications. XRD results show the transformation behavior of crystalline structures of different biomass ashes. Large amount of eutectic compounds generate thus lowered the melting point significantly.

The conventional ash fusion characteristic tested by sintering instrument cannot reflect the real conditions in industrial plants because of the high volatilization of biomass ash. Binary and ternary phase diagrams from silicate ceramics were employed to analyze the complex and changeable ash. The phase diagrams can be applied to obtain the fusion contribution of the related metal oxides. Moreover, the fusion properties of silica-rich biomass ash obtained by phase diagrams can be more appropriate for industrial running than the results from sintering instrument despite the limitations. In future work, efforts will be made to take into account the effect of chlorine and complement the analysis of silica-poor ash fusion properties with phase diagrams.

Acknowledgments

The authors wish to express the sincere thanks to the financial support from the National Basic Research Program (973 project: 2013CB228102) and the National Natural Science Foundation of China (51021065 and 50930006). The experiment was also assisted by Analytical and Testing Center of Huazhong University of Science and Technology. The constructive suggestions from Ms. Jingai Shao and linguistic help from Mr. Ho Simon Wang are also gratefully acknowledged.

Appendix A. Supplementary material

Supplementary data of the particle size distribution of the samples associated with this article can be found, in the online version, at http://dx.doi.org/10.1016/j.fuel.2013.07.085.

References

[1] Cornea TM, Dima M. Biomass energy – a way towards a sustainable future. Environ Eng Manage J 2010;9:1341–5.
[2] McKendry P. Energy production from biomass (Part 1): overview of biomass. Bioresour Technol 2002;83:37–46.
[3] McKendry P. Energy production from biomass (Part 2): conversion technologies. Bioresour Technol 2002;83:47–54.
[4] Jordan CA, Akay G. Speciation and distribution of alkali, alkali earth metals and major ash forming elements during gasification of fuel cane bagasse. Fuel 2012;91:253–63.
[5] Thy P, Jenkins BM, Grundvig S, Shiraki R, Lesher CE. High temperature elemental losses and mineralogical changes in common biomass ashes. Fuel 2006;85:783–95.
[6] Arvelakis S, Jensen PA, Dam-Johansen M. Simultaneous thermal analysis (STA) on ash from high-alkali biomass. Energy Fuels 2004;18:1066–76.

[7] Jensen PA, Frandsen FJ, Dam-Johansen K, Sander B. Experimental investigation of the transformation and release to gas phase of potassium and chlorine during straw pyrolysis. Energy Fuels 2000;14:1280–5.

[8] Knudsen JN, Jensen PA, Dam-Johansen K. Transformation and release to the gas phase of Cl, K, and S during combustion of annual biomass. Energy Fuels 2004;18:1385–99.

[9] Niu YQ, Tan HZ, Wang XB, Liu ZN, Liu HY, Liu Y, et al. Study on fusion characteristics of biomass ash. Bioresour Technol 2010;101:9373–81.

[10] Cha SC. Reactivity of ashes from biomass combustion plant in biomass combusting atmospheres. Mater Corros 2007;58:103–8.

[11] Lindstrom E, Sandstrom M, Bostrom D, Ohman M. Slagging characteristics during combustion of cereal grains rich in phosphorus. Energy Fuels 2007;21:710–7.

[12] Thy P, Jenkins BM, Lesher CE. High-temperature melting behavior of urban wood fuel ash. Energy Fuels 1999;13:839–50.

[13] Olanders B, Steenari BM. Characterization of ashes from wood and straw. Biomass Bioenergy 1995;8:105–15.

[14] Viana H, Vega-Nieva DJ, Torres LO, Lousada J, Aranha J. Fuel characterization and biomass combustion properties of selected native woody shrub species from central Portugal and NW Spain. Fuel 2012;102:737–45.

[15] Vamvuka D, Zografos D. Predicting the behaviour of ash from agricultural wastes during combustion. Fuel 2004;83:2051–7.

[16] Bryers RW. Fireside slagging, fouling, and high-temperature corrosion of heat-transfer surface due to impurities in steam-raising fuels. Prog Energy Combust Sci 1996;22:29–120.

[17] Huggins FE, Kosmack DA, Huffman GP. Correlation between ash-fusion temperatures and ternary equilibrium phase diagrams. Fuel 1981;60:577–84.

[18] Llorente MJF, Garcia JEC. Comparing methods for predicting the sintering of biomass ash in combustion. Fuel 2005;84:1893–900.

[19] Ogden CA, Ileleji KE, Johnson KD, Wang Q. In-field direct combustion fuel property changes of switchgrass harvested from summer to fall. Fuel Process Technol 2010;91:266–71.

[20] Arvelakis S, Folkedahl B, Dam-Johansen K, Hurley J. Studying the melting behavior of coal, biomass, and coal/biomass ash using viscosity and heated stage XRD data. Energy Fuels 2006;20:1329–40.

[21] Zevenhoven-Onderwater M, Backman R, Skrifvars BJ, Hupa M. The ash chemistry in fluidised bed gasification of biomass fuels. Part I: predicting the chemistry of melting ashes and ash-bed material interaction. Fuel 2001;80:1489–502.

[22] Wei X-L, Schnell U, Hein KRG. Behaviour of gaseous chlorine and alkali metals during biomass thermal utilisation. Fuel 2005;84:841–8.

[23] Nielsen HP, Baxter LL, Sclippab G, Morey C, Frandsen FJ, Dam-Johansen K. Deposition of potassium salts on heat transfer surfaces in straw-fired boilers: a pilot-scale study. Fuel 2000;79:131–9.

[24] Lin WG, Dam-Johansen K, Frandsen F. Agglomeration in bio-fuel fired fluidized bed combustors. Chem Eng J 2003;96:171–85.

[25] Arvelakis S, Jensen PA, Dam-Johansen M. Simultaneous thermal analysis (STA) on ash from high-alkali biomass. Energy Fuel 2004;18:1066–76.

[26] Baxter LL, Miles TR, Jenkins BM, Milne T, Dayton D, Bryers RW, et al. The behavior of inorganic material in biomass-fired power boilers: field and laboratory experiences. Fuel Process Technol 1998;54:47–78.

[27] Zaitsev AI, Shelkova NE, Lyakishev NP, Mogutnov BM. The thermodynamic properties of K_2O–SiO_2 melts. Russ J Phys Chem 2000;74:907–13.

[28] Forsberg S. Optimization of thermodynamic properties of the K_2O–SiO_2 system at high temperatures. J Phase Equilib 2002;23:211–7.

[29] Zaitsev AI, Shelkova NE, Mogutnov BM. Thermodynamics of Na_2O–SiO_2 melts. Inorg Mater 2000;36:529–43.

[30] Kirschen M, DeCapitani C, Millot F, Rifflet JC, Coutures JP. Immiscible silicate liquids in the system SiO_2–TiO_2–Al_2O_3. Eur J Mineral 1999;11:427–40.

[31] DeCapitani C, Kirschen M. A generalized multicomponent excess function with application to immiscible liquids in the system CaO–SiO_2–TiO_2. Geochim Cosmochim Acta 1998;62:3753–63.

[32] Steenari BM, Lindqvist O. High-temperature reactions of straw ash and the anti-sintering additives kaolin and dolomite. Biomass Bioenergy 1998;14:67–76.

[33] Hansen LA, Frandsen FJ, Dam-Johansen K, Sorensen HS. Quantification of fusion in ashes from solid fuel combustion. Thermochim Acta 1999;326:105–17.